Simulation of Surface-Moisture Effects on the Great Plains Low-Level Jet*

MICHAEL D. MCCORCLE

Department of Agronomy, Iowa State University, Ames, Iowa

(Manuscript received 3 September 1987, in final form 28 January 1988)

ABSTRACT

Convective precipitation and severe weather episodes in the central United States commonly have diurnal oscillations with maximum amplitudes at night. Observations suggest that the timing of some convective events may be driven by diurnal changes in the atmospheric boundary-layer convergence and vertical-motion fields resulting from a nocturnal, low-level jet over the southern Great Plains. Recent planetary boundary-layer models have attempted to simulate the strong boundary-layer forcings and dissipations that may be partly responsible for these low-level flows.

This research attempts to determine the effects of soil moisture and evaporation on the Great Plains nocturnal jet. Soil moisture determines surface evapotranspiration, latent heating, and soil thermal capacity and thereby plays an important role in the stratification and buoyancy of the boundary layer. Soil moisture should, therefore, be significant to this nocturnal, boundary-layer phenomenon.

This hypothesis is evaluated by embedding a soil hydrology system in a boundary-layer numerical model. A springtime case of nocturnal convection is analyzed, and data from this period are used to initialize the forecast model. Forecast experiments simulate well both nocturnal jets and vertical-velocity fields. In addition, the diurnal oscillations produced by the boundary-layer model are shown to be sensitive to surface moisture content and distribution.

1. Introduction

Despite great strides in short-range weather forecasting, the accurate prediction of spring and summer convective precipitation remains difficult. Many convective precipitation and severe weather episodes in the central United States have a distinct diurnal oscillation with maximum amplitude at night. Numerous cases of nocturnal convection enhancement have occurred during synoptic situations that seemingly destabilize the deep troposphere both day and night. Recent model development has been devoted to improving the forecast of both timing and location of these thunderstorm outbreaks. This study will report results of boundary-layer model simulations of a nocturnal-convection episode and will analyze the impact of surface moisture on boundary-layer processes.

Diurnal variabilities of late spring and summer precipitation and convection in the Great Plains have been well documented. Means (1952) analyzed July thunderstorm observations for stations in the central United States. The region from Oklahoma north to the Dakotas and east to the Mississippi River exhibited a nocturnal maximum in thunderstorm occurrence. Wallace (1975) compiled several years of hourly summer precipitation observations for more than 100 stations in the continental United States and constructed harmonic analyses of convective activity. As in Means' analysis, central regions of the Great Plains and the Mississippi Valley showed most frequent occurrence of convection near local midnight.

Observational work suggests that the timing of some convective events may be driven by diurnal changes in the atmospheric boundary-layer convergence and vertical-motion fields resulting from a nocturnal, low-level jet over the southern and central Great Plains. Observations by Blackadar (1957), Pitchford and London (1962), Bonner (1968), and Astling et al. (1985) suggest that low-level jets of the Great Plains typically are

(i) spring or summer phenomena,
(ii) located within 1 km of the ground,
(iii) found in a south to southwesterly ambient flow,
(iv) favored just upwind of convection, and
(v) transporters of significant amounts of water vapor.

Nocturnal jet activity is not confined to North America. Well-documented cases of jets are found in South America east of the Andes (Paegle 1984), east of the African highlands (Hart et al. 1978), and in Europe north of the Alps (Paegle et al. 1984).

* Contribution No. J-12804 of the Iowa Agriculture and Home Economics Experiment Station, Ames, Iowa. Project No. 2804.

Corresponding author address: Dr. Michael D. McCorcle, Climatology/Meteorology, 310 Curtiss Hall, Iowa State University, Ames, IA 50011.

Investigators have attributed these jets to

(i) diurnal oscillations of eddy viscosity (Blackadar 1957).
(ii) diurnal oscillations of buoyancy forces above sloping terrain (Holton 1967),
(iii) topographic flow-blocking due to increased nocturnal stratification (Paegle et al. 1984).

Because of the inability of most operational models to resolve boundary-layer phenomena, recent research has concentrated on the development of planetary boundary-layer models that are capable of simulating these nocturnal jets and resultant convergence fields. These models have attempted to accurately estimate the strong boundary-layer forcings and dissipations, which are believed responsible for these low-level flows. Paegle and McLawhorn (1983) developed a two-dimensional boundary-layer model that included a diurnal radiative cycle consisting of a surface energy budget and a dry-soil layer. Astling et al. (1985) performed tests of the model in three dimensions. The forecast results were successful in simulating nocturnal jets and synoptic-scale rising motion downwind of the wind maximum over the gentle slopes of the Great Plains.

The proposed mechanisms of the Great Plains nocturnal jet are dependent on diurnal changes in the thermal stratification of the boundary layer. Therefore, accurate estimates of the components of the surface energy balance are necessary to accurately predict low-level temperature fluctuations. Past modeling studies of this jet have partitioned all radiative energy reaching the bare surface to sensible heating of the atmosphere and dry-soil heat flux. No energy contributions from moisture in the soil and canopy have been simulated.

Surface moisture has two major contributions to the energy budget. Water augments the soil heat capacity and thermal conductivity, thereby increasing the soil's thermal stability. In addition, evaporation of soil moisture acts as a heat sink for sensible heat, and more of the surface energy is converted to latent heat. The combined effects of increased soil heat capacity and thermal conductivity, as well as latent heat exchange, on the diurnal temperature wave may significantly alter stratification, eddy viscosity, and buoyancy forces in the Great Plains boundary layer. McCumber and Pielke (1981) showed that changes in soil-moisture characteristics had a dramatic impact on surface temperature forecasts. They indicated that, for many soil types, an increase of soil-moisture content from approximately 25% to 75% of field capacity can damp the low-level diurnal temperature wave more than 5°C.

Horizontal discontinuities of soil moisture also may affect these boundary-layer events. Ookouchi et al. (1984) described results from model simulations which suggested that large horizontal gradients of soil moisture, resulting from past precipitation or variable climatological regimes, may produce significant horizontal variations in surface thermal forcing and thus may induce low-level atmospheric circulations.

This study will test the deterministic predictability of the low-level jet and associated diurnal oscillation of the vertical-motion fields by using the boundary-layer model described by Paegle and McLawhorn (1983), modified in this research to include soil-moisture prediction and evapotranspiration. With this addition, the study will test the response of the model to surface hydrology variables with a variety of model experiments. The model is described in section 2, and the soil-moisture treatment is presented in section 3.

To examine the model's ability to simulate observed jet phenomena, a springtime case of nocturnal convection is analyzed, and data from this period are used to initialize the forecast model. This case (the Tulsa Memorial Day Flood of 1984, 26–28 May 1984) was characterized by pronounced nocturnal thunderstorm activity over the central and southern Plains. Rawinsonde observations suggested a low-level wind oscillation during this period. The nocturnal maximum of the winds and the convection could not be explained by the large-scale synoptic situation.

Initial experiments to test the role of boundary-layer processes simulate dry soils. The forecast fields of horizontal winds and vertical velocities are examined to detect diurnal oscillations to compare with observations (section 5).

Several sensitivity experiments, presented in section 6, were performed to determine the effects of soil moisture. These tests introduce soil moisture over the horizontal domain by use of both homogeneous and heterogeneous initialization schemes. Experiments to determine the response of these boundary-layer flows to evapotranspiration from vegetation also are performed. Section 7 summarizes conclusions.

2. Model development

The boundary-layer model used in this study, although predominantly a three-dimensional form of the coupled earth–atmosphere model described by Paegle and McLawhorn (1983), has undergone several changes. The most important contribution from this research is the addition of a soil hydrology forecast system, which includes surface effects such as soil moisture and evapotranspiration. In this section, the details of the atmosphere, soil, and interface equations will be presented, followed by a brief description of the model numerics.

a. Atmosphere system

The atmospheric portion of the model is governed by an anelastic, hydrostatic system of equations. The equations in terrain-following, spherical coordinates (ϕ, λ, z) are

$$\frac{Du}{Dt} - fv = -\frac{1}{\rho_s a \cos\phi}\frac{\partial p'}{\partial \lambda} - \frac{g\rho'}{\rho_s a \cos\phi}\frac{\partial Z_T}{\partial \lambda} + \frac{\partial}{\partial z}\left(K_m \frac{\partial u}{\partial z}\right) + \nabla\cdot(K_d \nabla u) \quad (1)$$

$$\frac{Dv}{Dt} + fu = -\frac{1}{\rho_s a}\frac{\partial p'}{\partial \phi} - g\frac{\rho'}{\rho_s}\frac{1}{a}\frac{\partial Z_T}{\partial \phi} + \frac{\partial}{\partial z}\left(K_m \frac{\partial v}{\partial z}\right) + \nabla\cdot(K_d \nabla v) \quad (2)$$

$$\frac{\partial p'}{\partial z} = \rho' g \quad (3)$$

$$\rho\left[\frac{1}{a\cos\phi}\frac{\partial u}{\partial \lambda} + \frac{\partial}{\partial \phi}(v\cos\phi)\right] + \frac{\partial(w\rho)}{\partial z} = 0 \quad (4)$$

$$\frac{D\theta}{Dt} = \frac{Q}{C_p}\left(\frac{p_0}{p}\right)^{R/C_p} + \frac{\partial}{\partial z}\left(K_h \frac{\partial \theta}{\partial z}\right) + \nabla\cdot(K_d \nabla\theta) \quad (5)$$

$$\frac{Dq}{Dt} = \frac{\partial}{\partial z}\left(K_q \frac{\partial q}{\partial z}\right) + \nabla\cdot(K_d \nabla q) \quad (6)$$

$$p' = \rho' R T_{v_s} + \rho_s R T' + \rho' R T'. \quad (7)$$

Here, D/Dt is the terrain-following advective derivative, Z_T represents the terrain height, g is the gravitational force, a the earth's radius, f the Coriolis parameter, p the air pressure, and ρ is the air density. In the thermodynamic energy equation [Eq. (5)], θ is the potential temperature, Q the heating due to infrared radiative flux, p_0 is 1000 millibars, R is the gas constant for dry air, and C_p the specific heat capacity of air at constant pressure. Specific humidity, q, is the predictive quantity for atmospheric moisture. In the equation of state [Eq. (7)], T_v is the virtual temperature.

The pressure gradient and gravitational terms are rewritten in terms of standard thermodynamic variables (subscript s) and deviation thermodynamic variables (primed). The basic-state pressure field, which is assumed to vary only with height, is eliminated from the horizontal momentum equations, Eqs. (1) and (2). In addition, by assuming hydrostatic balance, the hydrostatic basic state is separated out of the vertical momentum equation [Eq. (3)]. Treatment of the thermodynamic variables in this manner reduces the truncation error of the horizontal pressure gradient term in the vicinity of sloped terrain as described in Paegle and McLawhorn (1983).

The vertical eddy-diffusion coefficient for motion, K_m, is given by

$$K_m = 0.2\alpha^{1/2} l. \quad (8)$$

The turbulent kinetic energy, α, is explicitly predicted by the model, and l is the vertical mixing length. The vertical eddy-diffusion coefficient for heat, K_h, is assumed equal to the diffusion coefficient for moisture, K_q, and is given by

$$K_h = K_q = 1.35 K_m, \quad (9)$$

where K_m is in units of $m^2\ s^{-1}$. The horizontal eddy-diffusion coefficient, K_d, is calculated as a function of the deformation rate, D, as in Smagorinsky (1963):

$$K_d = 0.36 D \Delta^2, \quad (10)$$

where Δ is the horizontal grid spacing.

The boundary-layer model uses a horizontal grid spacing of 1.875° by 1.875°. The horizontal domain is bounded by 5.625° to 54.375°N latitude, 71.25° to 120°W longitude, for a total of 27 by 27 horizontal grid points, covering most of the North American continent. An early ECMWF (European Centre for Medium-Range Weather Forecasting) operational topography is employed and smoothed with a nine-point operation (Shuman 1957) (Fig. 1). To account for the large vertical gradients of many of the prognostic variables at low levels of the atmosphere, a transformed grid system is used to increase resolution in the vertical. The lowest nine levels, below 119 m, use a logarithmically spaced grid. Above 119 m, 10 additional levels are equally spaced about 205 m apart, up to the top of the model at 2168 m above the surface. All results in this study and other investigations, including Astling et al. (1985), have indicated that observed boundary-layer oscillations over the Great Plains are confined below 1 km above the surface. Indeed, incorporating upper-tropospheric exchanges and a changing upper boundary may be important for some forecast details, but the current boundary-layer structure is deemed ad-

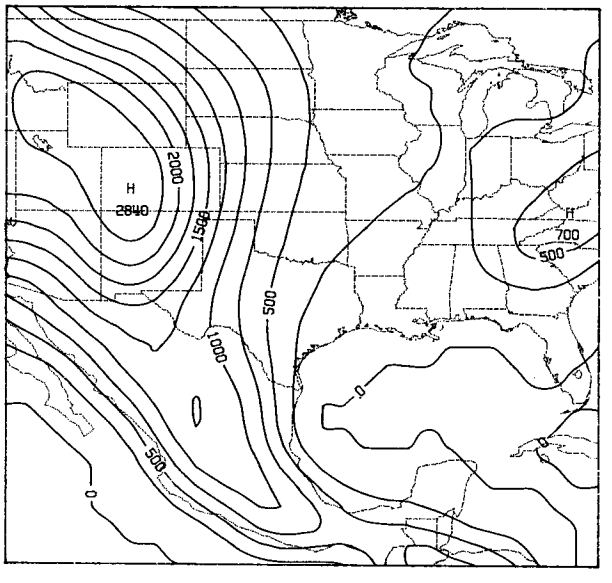

FIG. 1. Model topography (10^1 m). Contour interval is 250 m.

equate for the goals of this study, which emphasize a quasi-stationary synoptic situation.

b. Soil system

To more precisely predict surface forcings, the model incorporates forecasts of both moisture and heat fluxes within the soil by using a soil-moisture forecast method similar to that employed by the Air Force Geophysics Laboratory Soil Hydrology Model as described by Mahrt and Pan (1984) and Pan and Mahrt (1987). Connections between these moisture fluxes and atmospheric evaporation, as well as other details of the soil hydrology forecast, will be discussed in section 4.

The vertical grid consists of 15 soil-temperature computation levels, spaced equally 0.04 m apart, extending from the roughness height, z_0, at 0.04 m to 0.52 m below the surface. The soil hydrology model uses a two-layer method to update soil-moisture content. The upper layer is 0.08 m deep, and the lower layer is 0.96 m. Because temperature forecasts rely on soil-moisture content to calculate soil thermal conductivity and heat capacity, updated soil-moisture values are interpolated to match the soil-temperature forecast levels.

The transport of water in the soil can be described by the equation (e.g., Hillel 1980)

$$\frac{\partial \eta}{\partial t} = \frac{\partial}{\partial z}\left(D_\eta \frac{\partial \eta}{\partial z}\right) + \frac{\partial K_\eta}{\partial z} - E, \tag{11}$$

where η is the volumetric soil-moisture content and E is the change in moisture due to evapotranspiration or dewfall. The D_η is the soil diffusivity and K_η is the hydraulic conductivity, defined by

$$D_\eta = \frac{bK_{\eta_s}\Psi_s}{\eta_s}(\eta/\eta_s)^{b+3} \tag{12}$$

$$K_\eta = K_{\eta_s}(\eta/\eta_s)^{2b+3}. \tag{13}$$

The K_{η_s} and η_s are saturation values of hydraulic conductivity and soil-moisture content, respectively, Ψ_s is the saturation moisture potential, and b is a coefficient dependent on soil type. All these parameters are empirically defined as in Clapp and Hornberger (1978) and are soil-type dependent. For the top soil level, precipitation may be added to Eq. (12) but is not included in this research.

As in Zdunkowski et al. (1975), the soil-heat-flux equation is

$$C\frac{\partial T_s}{\partial t} = \frac{\partial}{\partial z}\left(\lambda_s \frac{\partial T_s}{\partial z}\right). \tag{14}$$

In this equation, T_s is the soil temperature, C the volumetric heat capacity of the soil, and λ_s the soil thermal conductivity. The thermal conductivity is a strong function of the moisture content and is calculated as in Al Nakshabandi and Kohnke (1965) by using the following relations:

$$\lambda_s = \exp[-(\log_{10}\Psi + 2.7)], \quad \text{for} \quad \log_{10}\Psi < 5.1 \tag{15}$$

$$\lambda_s = 0.00041, \quad \text{for} \quad \log_{10}\Psi > 5.1, \tag{16}$$

where λ is in units of cal s^{-1} cm^{-1} $°C^{-1}$ and Ψ is the soil-moisture potential, specified by the moisture content and soil type.

The volumetric heat capacity of the soil is estimated as a weighted function of the moisture content such that

$$C = (1 - \eta_s)C_i + \eta C_w. \tag{17}$$

In this relation, C_i is the heat capacity for the dry soil, and C_w is the heat capacity of water.

For the ocean, the thermal conductivity is defined as

$$\lambda_s(\text{ocean}) = \rho_w C_w K_w, \tag{18}$$

where ρ_w is the density of water, and K_w, the vertical-eddy-mixing coefficient, is chosen as 1.3×10^{-4} m^2 s^{-1} (Astling et al. 1985). This large value assures that sea surface temperatures are almost constant during the forecast period.

c. Interface conditions

Physical forcing in the model is due to radiative heating and cooling prescribed at the earth–atmosphere interface. The thermodynamic energy equation and soil-heat-flux equation are coupled with the surface heat-balance equation at the soil roughness height, z_0, to obtain the following:

$$G - F_n + \rho C_p K\frac{\partial \theta}{\partial z} - \lambda_s \frac{\partial T_s}{\partial z} - \rho_w L_v E = 0 \quad \text{at} \quad z = z_0. \tag{19}$$

where L_v is the latent heat of vaporization, and E is the evaporation rate in m s^{-1}. Solar (global) radiation, G, which appears in the surface energy budget equation, is calculated from

$$G = (1353 \text{ W m}^{-2}) \times (1 - A) \times \cos\theta_z, \tag{20}$$

where A is the albedo, which varies geographically according to summertime albedo datasets taken from Matthews (1985). The solar zenith angle, θ_z, is a function of latitude, time of day, and Julian day. The longwave (terrestrial) radiative flux, F_n, is calculated at the surface, and the atmospheric flux divergence, Q, appears as the heating term of the thermodynamic energy equation. These atmospheric fluxes are computed as functions of the water-vapor path length integrated through the atmosphere (see Paegle and McLawhorn 1983).

Temperature continuity is assumed at the roughness height such that

$$T_{\text{air}} = T_s \quad \text{at} \quad z = z_0. \tag{21}$$

A similar continuity relation exists for the moisture flux across the interface.

$$W_a = W_s \quad \text{at} \quad z = z_0. \tag{22}$$

The W_a and W_s are vertical moisture fluxes in the atmosphere and soil, and are given by the equations:

$$W_a = \rho K_q \frac{\partial q}{\partial z} \tag{23}$$

$$W_s = \rho_w E. \tag{24}$$

d. Boundary conditions and model numerics

The initial basic-state atmospheric temperature field is specified by assuming a vertical temperature lapse rate of 6.5°C km^{-1}. The basic state pressure and density fields are then determined from the equation of state. The pressure is specified at the top of the model. The initial wind field is assumed to be geostrophic above 200 m and logarithmically decreasing to zero at the roughness height. The upper-boundary condition maintains the initial pressure field, geostrophic wind, temperature, and specific humidity through the forecast period. At the bottom of the soil layer, the temperature is held constant. Lateral boundary conditions specify zero normal gradients or total reflection of all forecast variables.

In this study, all forecasts are initialized at the top of the model with an 850-mb height field representative of the specific case. By using the hydrostatic equation [Eq. (3)], this height field is converted into a pressure field for the model top. The forecasts are made for a 48-h period beginning from an initial time 0600 CST (1200 UTC).

Temperature, specific humidity, turbulent energy, and the horizontal wind are predicted in the model by using a prognostic equation of the form:

$$\frac{\partial A}{\partial t} + \mathbf{V} \cdot \nabla A = \frac{\partial}{\partial z}\left(K \frac{\partial A}{\partial z}\right) + F, \tag{25}$$

where A is the prognostic variable and F is the forcing, which includes the pressure gradient force and buoyancy effects. Typically, this type of equation is discretized by using various finite-differencing approaches. For results reported herein, the advection term, $\mathbf{V} \cdot \nabla A$, is approximated by using a leapfrog scheme. According to Paegle et al. (1976), finite difference approximations in z prove unstable for many profiles of K because of nonlinear computational instabilities. To overcome this problem, the right-hand side of Eq. (25) is discretized by use of a finite-element technique based upon Galerkin approximations. A detailed discussion of this method is found in Paegle and McLawhorn (1983). The vertical velocity is computed diagnostically and is calculated by integrating the continuity equation [Eq. (4)] by use of centered differencing. The pressure deviation, p', is determined by integrating the hydrostatic equation [Eq. (3)] downward.

3. Evapotranspiration simulation

Changes in thermal conductivity and heat capacity due to water in the soil require only minor adjustments in surface parameters. Contributions from evaporation to the heat balance and the moisture budget are more complex. Evaporation is not only a function of the incoming radiation, but also the three-dimensional wind field, the available soil moisture, and the atmospheric stability. In addition, when vegetation is present, transpiration from the plant stomata and evaporation from water on the plant surface may be important. Therefore, to completely determine the effects of surface moisture on boundary-layer phenomena, such as the nocturnal jet, a method to estimate evapotranspiration must be incorporated into the forecast model.

Deardorff (1977) determined that at least two soil layers, with a thin upper layer, are necessary to resolve evapotranspirative exchanges in an earth–atmospheric model. In such a system, surface evaporation is related to soil moisture near the interface whereas storage of soil water and transpiration are related to soil moisture in the deeper layer. Therefore, this forecast model incorporates a two-layer procedure to predict evaporative fluxes after the method used in Mahrt and Pan (1984). An overview of this method is presented below.

a. Potential evaporation

The total evapotranspiration from the soil surface includes evaporation from the bare ground, E_{dir}, transpiration from the vegetation, E_T, and evaporation from water accumulated on the canopy, E_c. The total evapotranspiration is given by

$$E = E_{\text{dir}} + E_t + E_c = FE_p. \tag{26}$$

In the model, all components of Eq. (26) are related to a function of the potential evaporation, E_p, defined as the evaporation from a well-watered surface under a given set of atmospheric conditions. The F is a function relating to variables such as soil-water distribution, plant density, stomatal resistance, vegetation type, and canopy-water content.

The potential evaporation is a function only of atmospheric variables and is determined from a formulation (Penman 1948), which has been modified to include the effects of variable atmospheric stability. The relation uses a surface energy balance derived from bulk aerodynamic relationships for the heat and moisture fluxes. The potential latent-heat flux, W_p, is given by

$$W_p = \frac{B(G - F_n - S)}{1 + B} + \frac{\rho L_v C_q u(q^* - q)}{1 + B}, \tag{27}$$

where

$$B = \frac{0.622}{p} \frac{L_v}{C_p} \frac{de^*(T)}{dT}, \tag{28}$$

$$S = \lambda_s \frac{\partial T}{\partial z}. \tag{29}$$

Here S is the soil heat flux and e^* the saturation vapor pressure at temperature T. The T, ρ, p, q and q^* are the temperature, air density, air pressure, specific humidity, and saturation specific humidity at a height of about 2 m above the surface; C_q is the nondimensional exchange coefficient for moisture, a function of the Richardson number. The right-hand side of Eq. (27) consists of two terms that represent radiation (first term) and aerodynamic effects (second term) on evaporation. The potential evaporation is then calculated from the relation:

$$E_p = \frac{W_p}{\rho_w L_v}. \tag{30}$$

b. Direct evaporation

The direct evaporation from bare soil is estimated by assuming that evaporation proceeds at the potential rate until the soil-moisture content of the upper layer decreases to an "air-dry" value (Nimah and Hanks 1973). At this point, the water film on soil particles is considered to be so thin that electrostatic forces prevent evaporation from proceeding at the potential rate. This air-dry value of soil-moisture content is dependent on soil type only. Therefore, the bare-soil evaporation is estimated by the following method.

If $\eta_{\text{sfc}} > \eta_d$:

$$E_p = E_{\text{soil}} = E_p \quad \text{at} \quad z = z_0. \tag{31}$$

If $\eta_{\text{sfc}} < \eta_d$:

$$E_{\text{soil}} = D_\eta \frac{\partial \eta}{\partial z} + K_\eta < E_p. \tag{32}$$

If vegetation is included, the direct evaporation from the soil is defined by the equation:

$$E_{\text{dir}} = E_{\text{soil}}(1 - \sigma_f). \tag{33}$$

Vegetation reduces direct bare-soil evaporation by shading the bare soil and reducing the wind speed near the ground. Both these influences are related to the shading factor, σ_f, a value that ranges from 0 to 1; $\sigma_f = 0$ signifies no foliage, and $\sigma_f = 1$ representing complete radiative blocking. The shading factor varies from 0.4 to 0.9 for most biomes and is assumed a value of 0.7 for the vegetation sensitivity tests discussed in section 6.

c. Canopy evaporation

The amount of water captured and retained by vegetation and evaporated back to the atmosphere without adding moisture to the soil is defined as the canopy evaporation. The time rate of change of canopy-water storage, c_a, is directly proportional to the canopy evaporation and is updated from the equation:

$$\frac{dc_a}{dt} = -\sigma_f (c_a/s)^{1/2} E_p = -E_c, \tag{34}$$

where s is the storage capacity of the canopy. For a short-grass vegetation, as is assumed in this research, the storage capacity is estimated to be 1.3 mm (Zinke 1967).

d. Transpiration

Transpiration is related to the soil-moisture content, the density of vegetation cover, and the stomatal, internal, and root resistance of the vegetation. In addition, the presence of canopy water reduces transpiration. All these effects are included in the equation:

$$E_t = E_p k_v \sigma_f \left[\left(\frac{\Delta z_1}{\Delta z_1 + \Delta z_2} \right) h(\eta_1) + \frac{\Delta z_2}{\Delta z_1 + \Delta z_2} h(\eta_2) \right] [1 - (c_a/s)^{1/2}] \tag{35}$$

$$h(\eta) = \begin{cases} 1, & \text{if} \quad \eta > \eta_{\text{ref}} \\ \dfrac{\eta - \eta_{\text{wilt}}}{\eta_{\text{ref}} - \eta_{\text{wilt}}}, & \text{if} \quad \eta < \eta_{\text{ref}} \\ 0, & \text{if} \quad \eta \leqslant \eta_{\text{wilt}} \end{cases} \tag{36}$$

where η_1 and η_2 are the soil-moisture contents of the top and bottom soil layers, respectively, and E_p is the potential evaporation. The wilting point, η_{wilt}, is defined as the moisture content at which root uptake ceases, and the reference moisture content, η_{ref}, is that moisture content at which soil-moisture deficit begins to reduce uptake. These values are soil-texture-type dependent. The product of $\sigma_f k_v$ is called the plant coefficient and is assumed to have a late springtime value of 0.7. This expression for transpiration assumes that the root uptake is independent of the depth of the given layer.

4. Case description

Model performance and soil-moisture sensitivity were tested by using a springtime synoptic case, when nocturnal maxima of convection and a low-level jet occurred over the central Great Plains. Data from this case then were used to initialize the numerical prediction model. Details of the synoptic situation surrounding this case are described in this section. Rainfall data and other storm data were taken from *Hourly Precipitation Data* and *Storm Data,* publications of the National Weather Service, U.S. Department of Commerce.

Very heavy rains, associated with a nocturnal thunderstorm complex, fell over central portions of the Great Plains from the late evening on 26 May 1984 to the early morning of 27 May. As depicted in Fig. 2a, rainfall during this period exceeded 2.5 cm over a large portion of northeastern Oklahoma and northwestern Arkansas. The precipitation in the Tulsa metropolitan

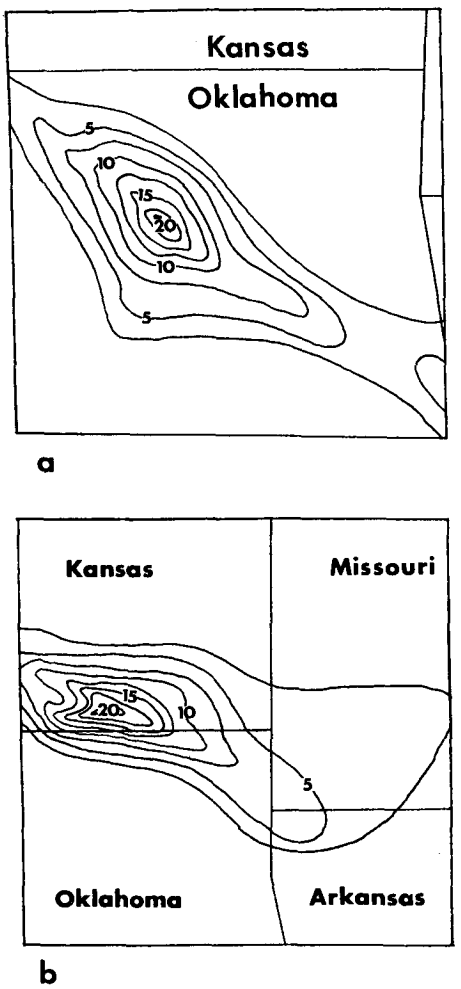

FIG. 2. Rainfall (cm) (a) over northeastern Oklahoma from 2000 CST 26 May 1984 to 0500 CST 27 May (0200–1100 UTC) and (b) over southeastern Kansas from 0300 to 1100 CST 27 May (0900–1700 UTC).

area, as shown in Fig. 3, exceeded 20 cm and was heaviest near 0000 CST (Central Standard Time, or 0600 UTC). The thunderstorm complex spawned tornadoes, hail, and damaging winds, as well as flooding. Later that night, the convective activity increased again, with many regions of southeastern Kansas reporting heavy rains and other forms of severe weather. Figure 2b shows that rainfall in some locations, once again, exceeded 20 cm. By midmorning, nearly all of northeastern Oklahoma, eastern Kansas, and western Missouri had received at least 1 cm of precipitation. The convection subsided during the daytime hours of 27 May, but scattered thunderstorms formed again after midnight from northeastern Kansas to northern and central Arkansas. Heaviest rainfall amounts of 2 to 4 cm fell between 0000 and 0600 CST 28 May over portions of east-central Arkansas north to the Missouri border.

A very persistent, southerly low-level flow and a stationary surface front south of the area provided the synoptic support necessary for the convective activity. The surface-pressure fields and surface frontal zones for 1200 UTC 26–28 May are shown in Fig. 4a–c. On 26 May, a cold front extended from a surface low-pressure center, north of the Great Lakes, southward through central Arkansas into northern Texas. On 27 May, the same front was analyzed as stationary and had moved slightly northward. The front began to move south and east on 28 May in response to an upper-level disturbance that moved eastward across the region.

The evolution of the 500-mb height field, depicted in Fig. 4d–f for 1200 UTC 26–28 May, shows a very weak zonal flow over the Southern Plains for the first 2 days of the period. On the 28th, the flow amplitude increased, and a shortwave trough deepened into the Central Plains. Lack of a meridional ambient flow component during most of this period was responsible for the persistent nature of the east–west oriented surface front.

At 850 mb, southerly winds were common over much of the Central and Southern Plains because of a low-level cyclone that developed on the front range of the Colorado Rockies and slowly moved across the area during the period. Warm air, moving northward with this flow, was forced to rise over the cool dome of air, bounded by the stationary front, thus favoring upward motion and convection. The 850-mb height fields for 0000 and 1200 GMT 27 May are shown in Fig. 5. These 850-mb figures show pronounced nocturnal wind accelerations from rawinsonde observations taken at Dodge City (DDC), Amarillo (AMA), Oklahoma

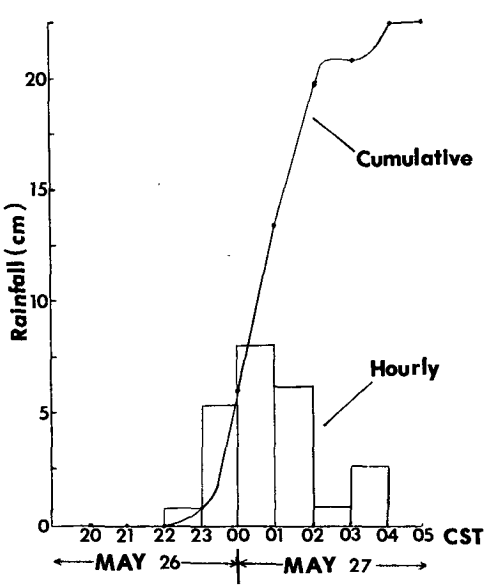

FIG. 3. Hourly and cumulative rainfall (cm) for the Tulsa International Airport, 26–27 May 1984.

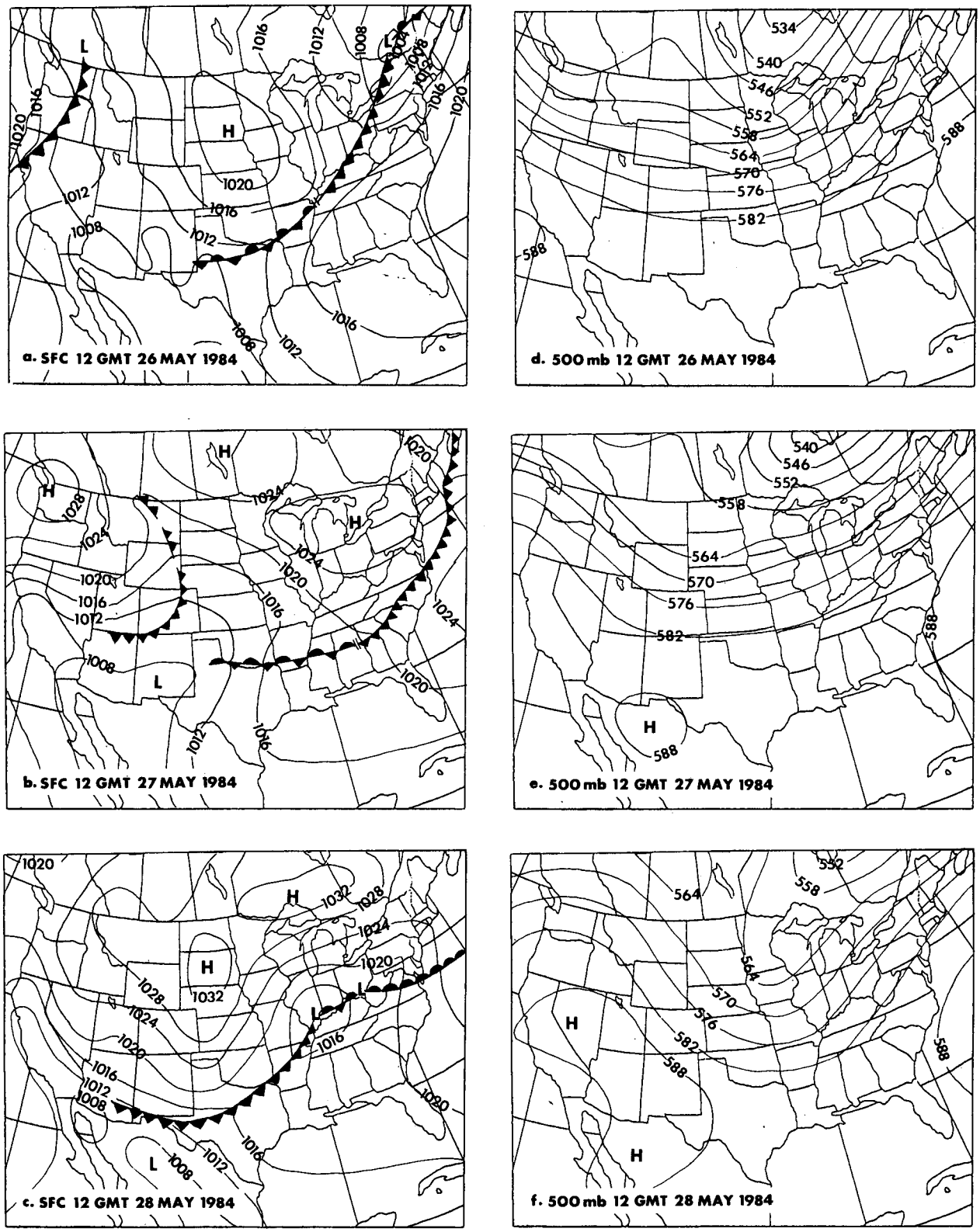

FIG. 4. The evolution of the surface pressure field (mb) and the 500-mb height field (10^1 m) from 1200 UTC 26 May 1984 to 1200 UTC 28 May 1984.

City (OKC), and Midland (MAF). At 0000 UTC 27 May, all four of these stations reported wind speeds of 10 m s^{-1} or less. By 1200 UTC, these wind speeds had doubled, with little observable change in the height gradient. For example, the Oklahoma City wind speed at 1200 UTC was 20 m s^{-1} compared with only 7.5 m s^{-1}, 12 hours earlier.

This particular case is chosen, not only for its nocturnal maxima of wind and precipitation, but also for the soil conditions present. Until this period of convection, much of the southern Great Plains had experienced very little spring precipitation. As shown in Fig. 6, in the vicinity of the low-level jet, the southern Great Plains, and westward over the Rockies, most regions were reporting low soil-moisture conditions. For this reason, this case seemed appropriate for testing whether these dry soil conditions had any affect on the observed jet activity.

5. Dry soil simulation

An 850-mb height field representative of the flow during the 2-day convective period, 1200 UTC 27 May 1984 (Fig. 5b), was used to initialize the boundary-layer forecast upper-boundary condition. This is the closest available observation time with respect to the heavy rains. Its selection is motivated by the desire to understand what the boundary-layer model response would be in a setting that provided accurate upper-boundary data at the time of greatest weather activity. Because the present case is only slowly evolving on the synoptic scale, it is unlikely that results initialized from previous-afternoon data would be much different. Model soils were assumed dry and bare. A 48-h forecast was made to allow a clear demonstration of boundary-layer oscillations. Horizontal and vertical velocity results in Figs. 7 and 8 are taken from forecast results from 1400 and 0200 CST, the time periods that coincide with minimum and maximum jet activity in the model.

The level of the jet core in the model is near 500 m above the ground. Forecast winds at this level for each nocturnal period (0200 CST) are shown in Figs. 7a–b. A strong southerly jet is evident in both figures. Wind speeds forecast for both nights exceed 24 m s^{-1} over southwestern Texas and are at least 12 m s^{-1} over much of the southern Plains. Farther north, the winds quickly decelerate to less than 10 m s^{-1} over northern Kansas and Missouri. The diurnal oscillatory behavior of the jet is demonstrated in Figs. 7c–d. In these depictions, the 500-m velocity field at 1400 CST is subtracted from the nighttime field, at 0200 CST. For the first forecast day, wind speeds at night exceed afternoon speeds in southwestern Texas by nearly 14 m s^{-1}, and by at least 6 m s^{-1} over much of the Southern Plains. A similar pattern is seen for the second day inasmuch as nocturnal wind speeds were almost double their daytime values over Texas, Oklahoma, and Arkansas. A secondary maximum in wind differences is present over northeastern Oklahoma.

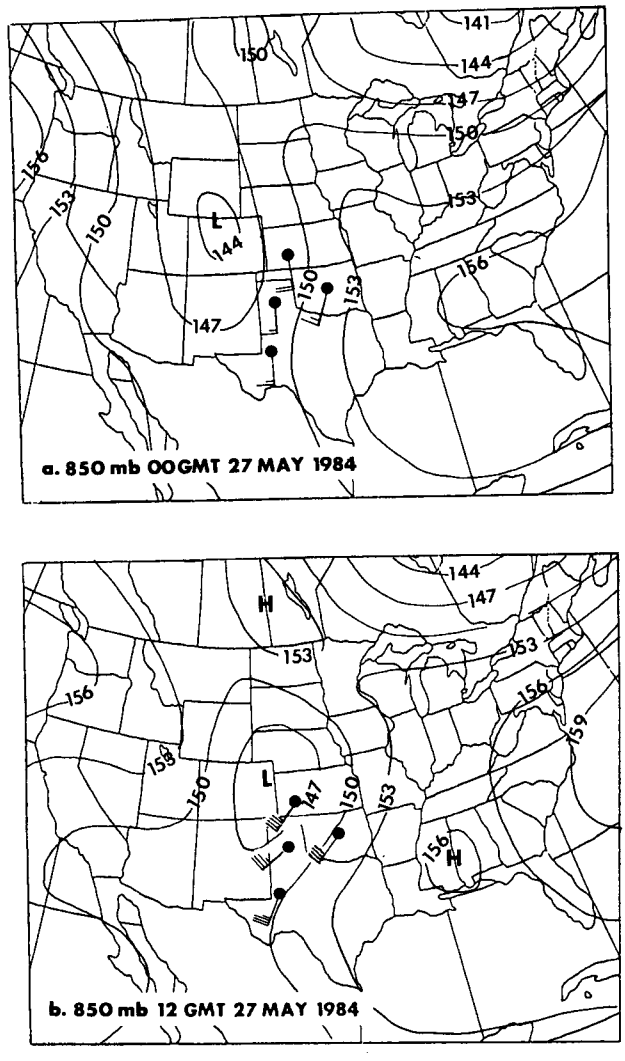

FIG. 5. The 850-mb height field (10^1 m) with selected wind observations for (a) 0000 UTC 27 May 1984 and (b) 1200 UTC 27 May 1984. Full wind barb equals 5 m s^{-1}.

These speed decelerations ahead of the jet over northern Oklahoma, northern Arkansas, southern Kansas, and southern Missouri produce nocturnal boundary-layer convergence, which closely matches the areas of observed storm activity. As shown in Fig. 8a–b, this convergence produces rising motion at the top of the boundary layer, which exceeds 2 cm s^{-1} over eastern Oklahoma on the first forecast night and is greater than 3 cm s^{-1} over southeastern Kansas the second night. Vertical-velocity-difference fields are depicted in Figs. 8c–d. Figure 8d shows that nocturnal rising motions the second night exceeded daytime vertical velocities by more than 4 cm s^{-1} over the areas of observed convection. Also noteworthy are the negative fields forecast over the Rockies, which demonstrate daytime maxima in rising motion resulting from daytime heating of the slopes. These results suggest that

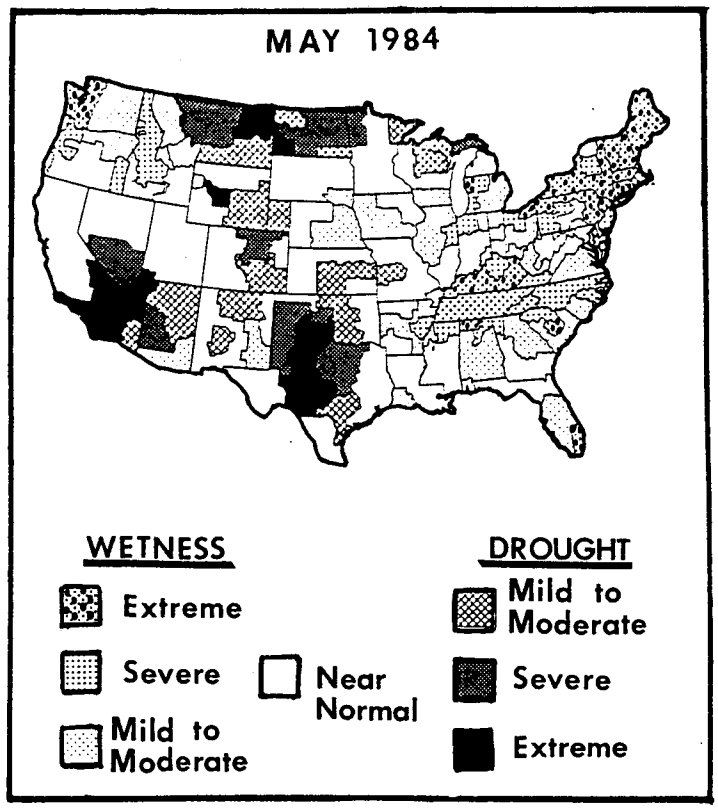

FIG. 6. Palmer Drought Severity Index for May 1984.

a strong trigger for convection may be present at the top of the Great Plains nocturnal boundary layer that is not evident during the heat of the day.

The diurnal oscillation of forecast vertical velocities for two gird points is plotted in Fig. 9. One point is located in extreme southwestern Missouri, near the area of observed nocturnal convection, and the other in southern Colorado in the Rocky Mountains. These vertical velocity plots are nearly 180 degrees out of phase. For the point in Missouri, positive vertical motions show definite nocturnal maxima near 0200 CST both nights, whereas the point in the Rockies has peak rising motions near 1400 CST.

It is likely that diurnal oscillations in the boundary layer, as strong as those forecast by the model, could phase nocturnally synoptic-scale convection. These forecast results are not merely isolated successes. Anthes et al. (1982) and Astling et al. (1985) also have successfully predicted low-level convergence fields in vicinity of low-level jets and heavy convection.

6. Surface sensitivities

a. Soil moisture

The same synoptic case is used to test the model's sensitivity to varying the soil-moisture content. Three experiments were performed with increasing soil moisture initialized homogeneously over all land areas: (i) $\eta = 0$, dry soil (results discussed in Chapter 6), (ii) $\eta = 0.75\eta_s$, and (iii) $\eta = \eta_s$, complete saturation.

In Fig. 10, the 529-m wind-speed maxima are plotted as a function of forecast time for each case. As soil moisture increases, the amplitude of the predicted diurnal wind modulation decreases. Results from the saturated-soil case reveal a 40% decrease in the jet speed over the dry-soil case. Figure 11 shows the vertical-velocity-difference fields at the top of the model for the forecast with saturated soil. The Great Plains nocturnal vertical velocities exceed daytime values by less than 2.0 cm s^{-1} on the first forecast day and 2.8 cm s^{-1} on the second day. This compares with 3.3 and 4.2 cm s^{-1}, respectively, for the dry case (Figs. 8c, d).

The forecasts of vertical velocities at two grid points, for these three cases, are shown in Fig. 12. The points were the same as those chosen in Fig. 9, one located in Missouri and the other in the Colorado Rockies. Damping of the amplitude of the diurnal oscillation for the wetter soils is evident in both figures. For the grid point in the Plains, the diurnal oscillation of rising motion for the saturated case is nearly half that of the dry case. These results suggest that the observed dry soils present over the Great Plains and the Rockies during the case period may have enhanced jet activity and boundary-layer convergence.

The effect of soil moisture on wind speeds and resulting vertical velocities may, in part, be attributed to decreased low-level buoyancy along the sloping terrain. Holton (1967) suggested that the diurnal temperature oscillation near the surface of the Great Plains provides a source of potential energy that drives a diurnal oscillation in the boundary-layer winds. In this theory, nocturnal convergence develops as a buoyancy-driven wind vector, directed upslope during the day, is turned clockwise by the Coriolis force, and aligns with the southerly ambient flow. Consequently, the strength of this jet-forming mechanism is directly related to the amplitude of the diurnal temperature wave. Above moist soils, diurnal temperature changes are reduced, as more available energy is partitioned to evaporation and soil heat flux, which is increased due to the higher conductivity of the moist soil. As a result, this buoyancy-driven component of the jet is diminished as soil moisture increases, thereby decreasing nocturnal convergence over the Great Plains.

Soil moisture shows great geographic variability depending on precipitation history, atmospheric humidity, soil type, and vegetation. Therefore, heterogeneous soil moisture initialization may be necessary to achieve precision in this type of forecast. To test this possibility, two heterogeneous initialization experiments are examined. As shown in Fig. 13, the first experiment was performed with saturated soil conditions in the Southern Plains downwind of the jet core, and all other land areas are assumed dry. In the second test, only the soils of the Southern Rockies are initially saturated.

Figure 14 shows the vertical-velocity-difference field for the second forecast day of these tests. In the first case, the addition of soil moisture to the Southern Plains results in an increase in nocturnal rising motion. The nighttime rising motion exceeds daytime values by more than 5.2 cm s^{-1}. This compares with 4.1 cm s^{-1} for the homogeneous dry case. This response is almost twice as strong as in the case that had all land regions initialized with saturated soils.

Different results are obtained in the second experiment. With wet Rocky Mountain soils, the forecast diurnal change in vertical velocity over the Great Plains is only 3.1 cm s^{-1}, nearly 25% less than the homoge-

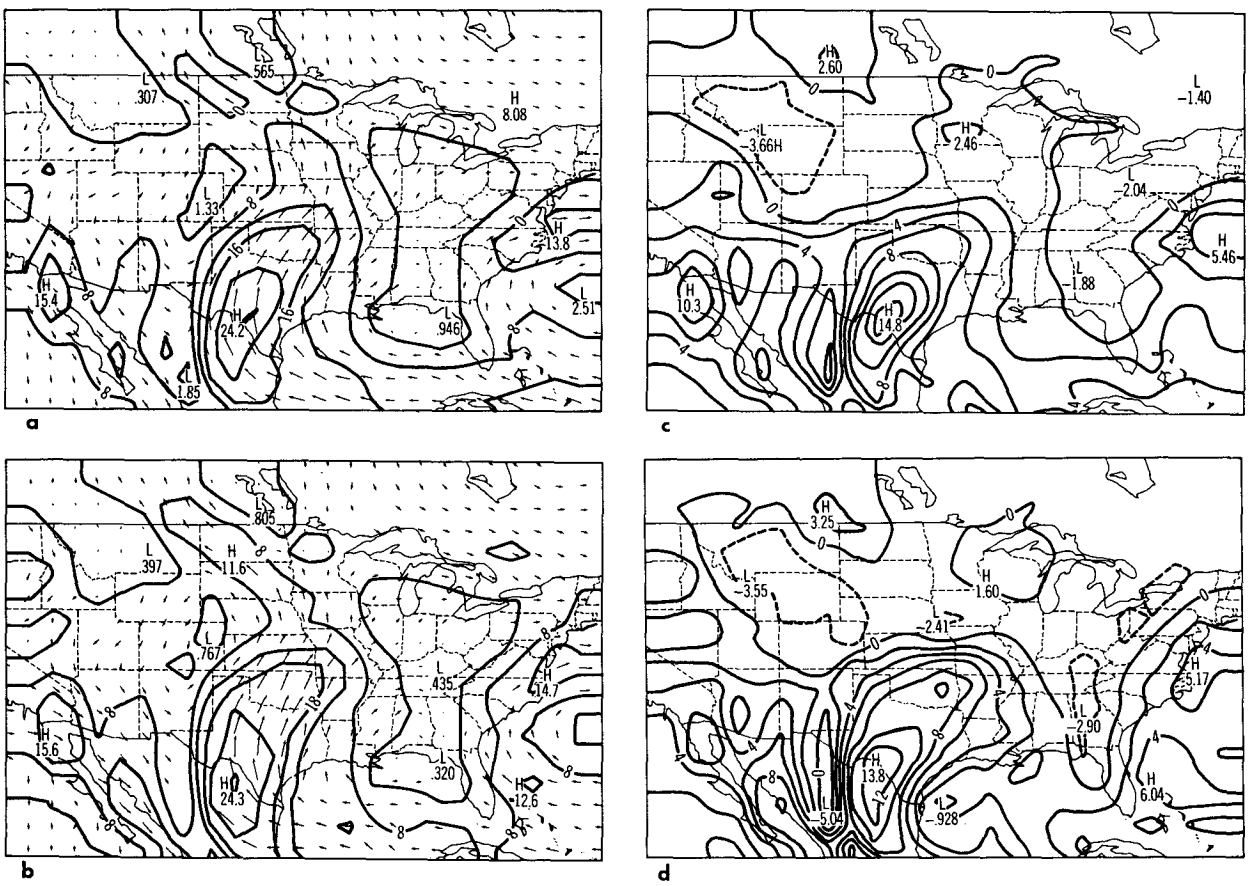

FIG. 7. Dry soil simulation. Forecast 500-m wind field and isotachs (m s^{-1}) for (a) 0200 CST, the first forecast day and (b) 0200 CST, the second forecast day. Contour interval is 4 m s^{-1}. (c) Horizontal-velocity-difference field, 0200 CST minus 1400 CST for the first forecast day. Solid contours denote positive values and dashed indicate negative quantities. Contour interval is 2 m s^{-1}. (d) As in (c) but for the second day.

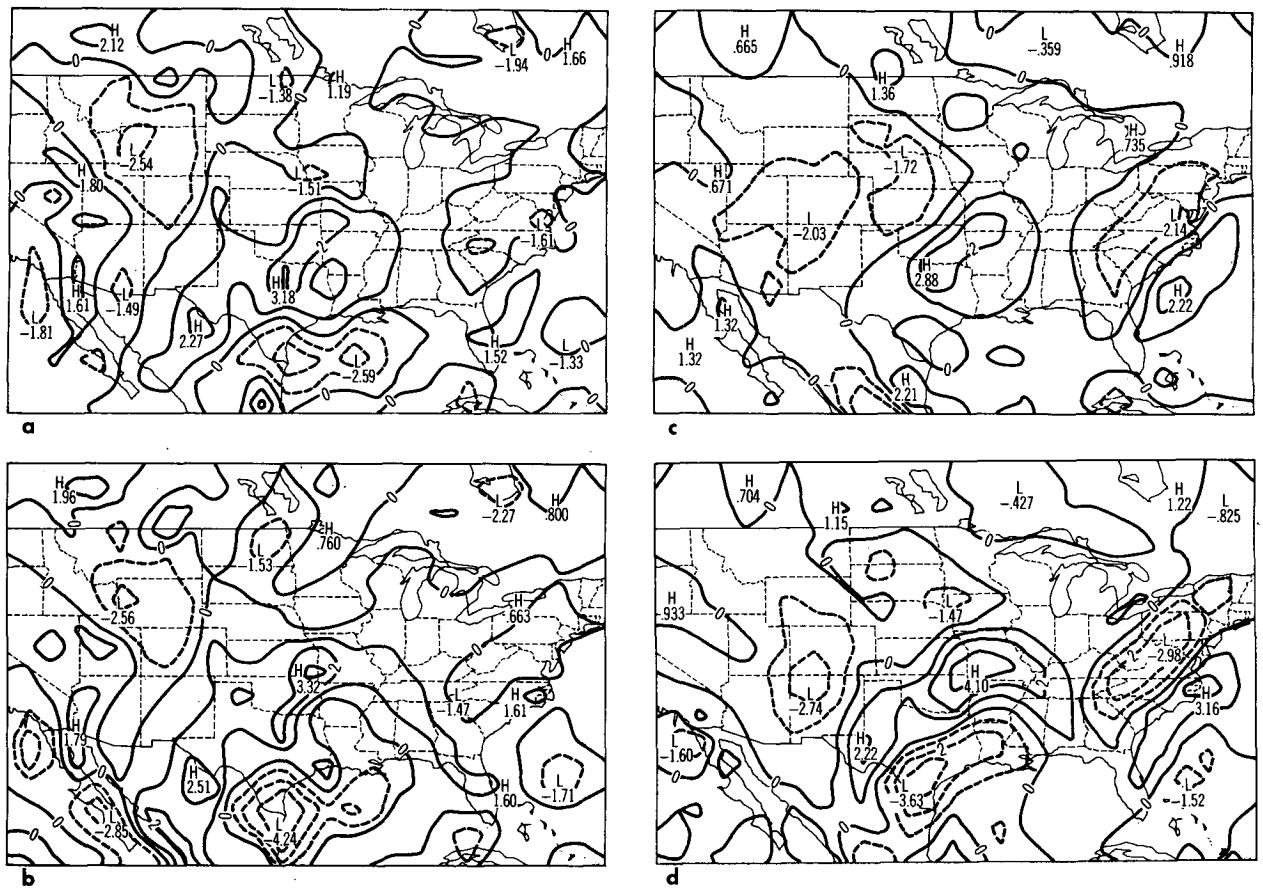

FIG. 8. Dry soil simulation. Forecast vertical velocity field at 2168 m (cm s^{-1}) for (a) 0200 CST the first forecast day and (b) 0200 CST, the second forecast day. Contour interval is 1 cm s^{-1}. Solid lines denote upward motion, and dashed lines indicate downward motion. (c) Vertical-velocity-difference field, 0200 CST minus 1400 CST, the first forecast day. Contour interval is 1 cm s^{-1}. Solid contours are positive and dashed are negative. (d) As in (c) but for the second day.

neous dry case. Saturating the mountain soils had comparable results to saturating all land regions where the diurnal vertical-velocity difference was reduced to 2.8 cm s^{-1}.

The results of these two experiments indicate that the gradient of soil moisture along the east–west slopes of the Rockies may strongly affect the nocturnal jet and associated rising motion. These conclusions agree with Ookouchi et al. (1984) who demonstrated, on a

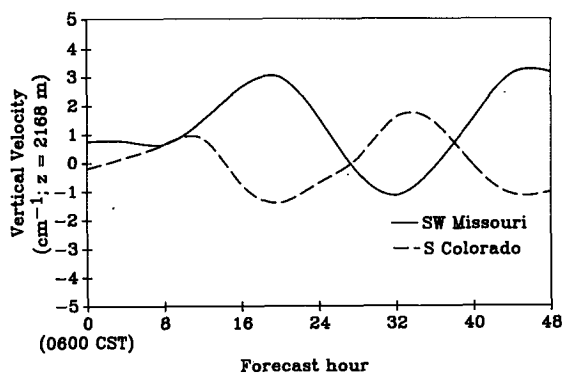

FIG. 9. Vertical velocity forecast (cm s^{-1}) at 2168 m for grid points in southwest Missouri (solid) and southern Colorado (dashed) for the dry soil case.

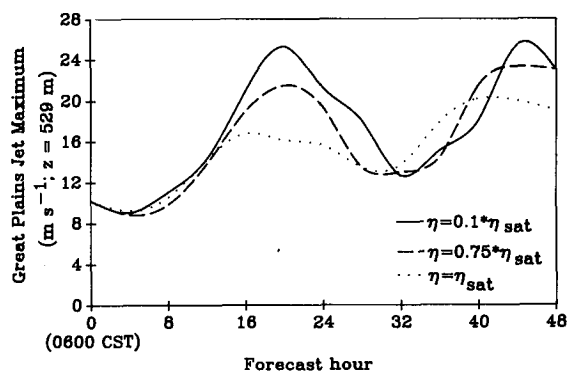

FIG. 10. Forecast wind-speed maxima at 500 m versus forecast time for the wet soil experiments.

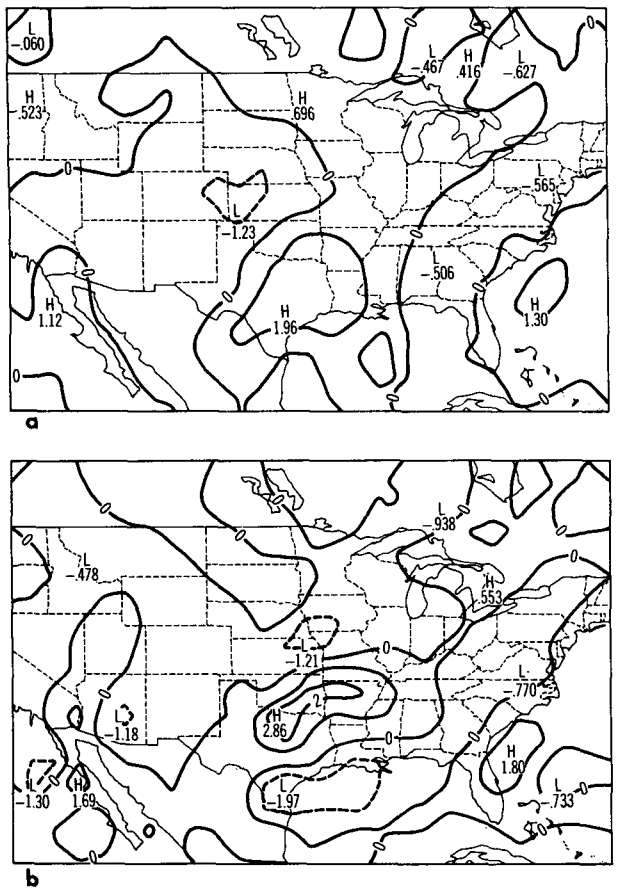

FIG. 11. Saturated soil (homogeneous). Vertical velocity-difference field, 0200 CST minus 1400 CST, for (a) the first day of forecast and (b) the second day of forecast. Contour interval is 1 cm s^{-1}.

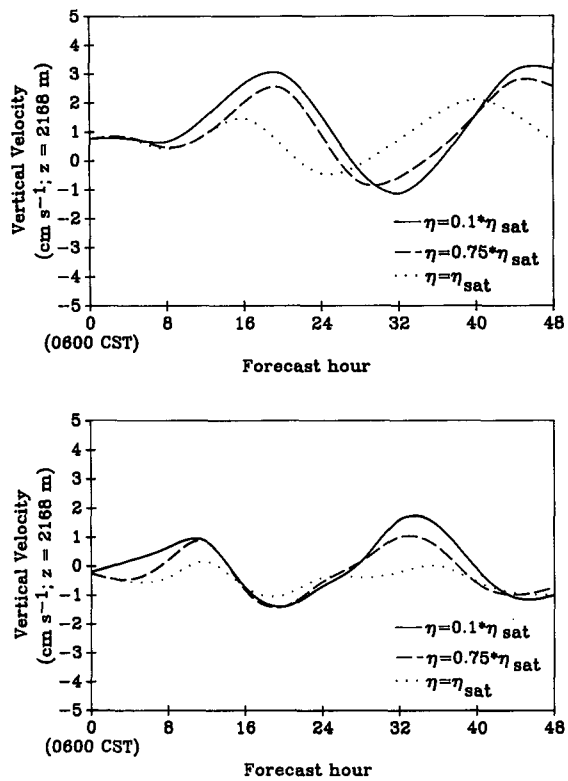

FIG. 12. Vertical velocity forecasts (cm s^{-1}) at 2168 m for grid points in (a) Missouri and (b) Colorado for the wet soil experiments.

smaller horizontal scale, that a thermally-direct circulation, which develops above the boundary between wet and dry soils, may counteract or augment buoyant slope circulations. In the first model experiment, with the lower elevations saturated, the circulation that evolves at the moisture boundary is in phase with the slope-induced circulations and thus increases the ageostrophic component. The inertial turning of these coupled circulations results in greater nocturnal wind speeds and enhanced boundary-layer convergence over the Great Plains. Conversely, saturated soils at higher elevations, as in the second case, produce a thermally-direct circulation that counteracts the buoyancy-driven oscillation, resulting in reduced jet speeds and decreased rising motion.

The response of the boundary-layer model in these experiments suggests the potential importance of including spatial distributions of soil moisture in forecast initialization.

b. *Vegetation*

Assuming a homogeneous soil-moisture content ($\eta = 0.75\eta_s$) and again initializing the model with data from 1200 UTC 27 May 1984, two experiments are performed, varying the vegetative conditions in each. The first test assumes a short-grass vegetation with 70% coverage of the bare soil surface. The evaporation components of this test include direct soil evaporation as well as grass transpiration. The second experiment assumes the same vegetation with the addition of canopy water. The amount of water on the canopy is in-

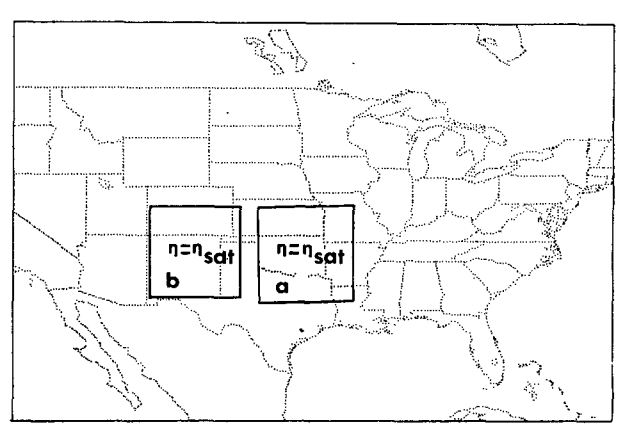

FIG. 13. Heterogeneous soil-moisture initialization regions. Region **a** was saturated for test with wet soils in the Plains and region **b** was saturated for test with wet soil in the Rockies.

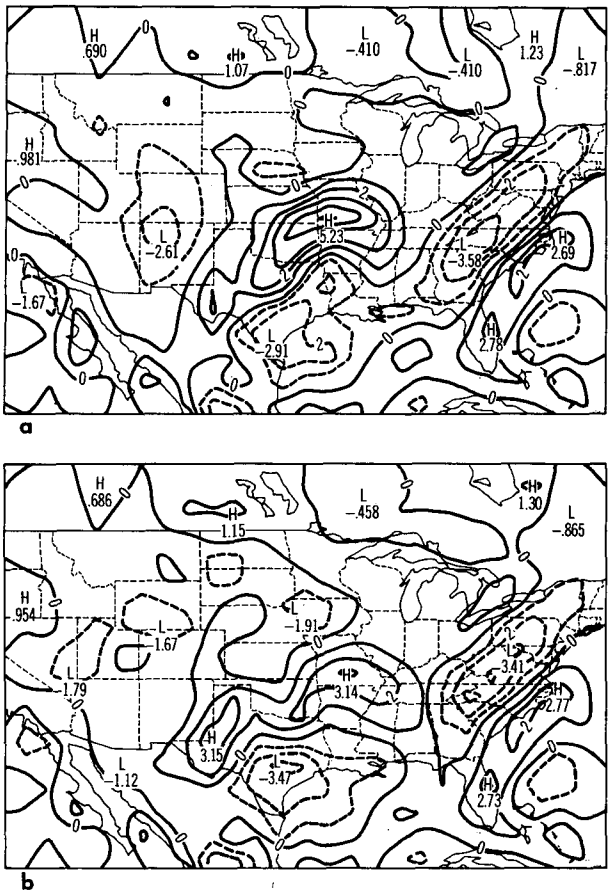

FIG. 14. As in Fig. 11b for (a) wet soils in the Plains and (b) wet soils in the Rockies.

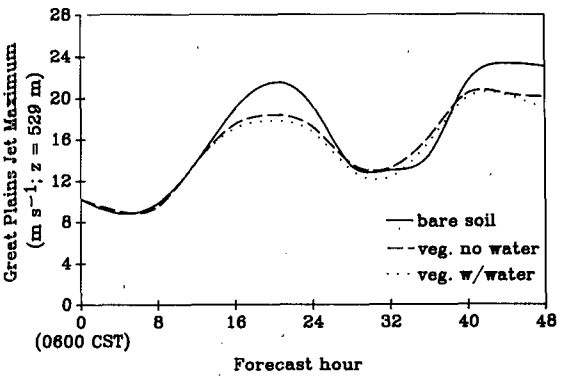

FIG. 15. As in Fig. 10, for vegetation simulation cases.

itialized at 50% of the water capacity of short-grass vegetation, which from Zinke (1967) is 13 mm.

These test results are compared with the bare-soil experiment described in the last section, using a plot of the wind-speed maxima versus time, shown in Fig. 15. The tests with vegetation decrease the forecast nocturnal wind-speed maximum by about 4 m s^{-1} over the bare-soil case. These lower speeds result in 5% reductions of diurnal differences in vertical velocity downwind of the jet. The model shows little sensitivity to the canopy moisture test. In both cases, the total evapotranspiration is approximately the same as the bare-soil case. The transpiration from the canopy taps moisture from the lower-soil layer, however, the groundcover reduces bare-soil evaporation from the surface, causing the upper-soil layer to retain more moisture through the forecast period. As a result, the wetter soils decrease the diurnal temperature variation with respect to the bare-soil case, consequently damping the buoyant oscillation.

The rather weak responses to these vegetation parameters may be partly due to limiting model evapotranspiration to the potential-evaporation rate. Actual evapotranspiration often exceeds the potential rate in cases of strong warm advection at the surface. Development of a heat budget for the canopy is needed before further evaluation of the role of vegetation can be made.

c. *Soil parameters and forecast initialization*

If a soil-hydrology prediction method, such as the one described in this research, is to be used in an operational environment, questions regarding the initialization of soil-moisture content must be addressed. Soil water values are not reported on a consistent basis in the United States, mostly because of the cost of instrumentation and manpower. However, estimates of crop-moisture availabilities are made on a weekly basis in the central United States by using an empirical value known as the crop-moisture index. This parameter is a function of rainfall, time of year, vegetation type, and other factors. It might be possible, using this type of index, to estimate relative soil-moisture contents to a degree adequate for a boundary-layer simulation.

Another initialization problem is soil-type specification. Parameters such as soil-moisture field capacity, wilting point, heat capacity, etc., are highly soil-type dependent. The soil texture types of sands, loams, and clays show great variability over very small regions. It is not clear whether heterogeneous soil type information could be accurately represented for a horizontal grid as large as the one used here. Further research and testing is necessary.

7. Summary

The diurnal oscillation of convective events in the Great Plains of North America has been documented by investigators for many years. Their findings have shown that the nocturnal phasing of convection may occur even when the large-scale synoptic situation would warrant convection both day and night. Most theories have attributed these diurnal oscillations to changes in boundary-layer convergence fields resulting from a low-level nocturnal jet. Convergence in the re-

gion downwind of this jet may result in strong upward vertical motion at the top of the boundary layer. Recent studies have been devoted to simulating these oscillatory characteristics in a boundary-layer forecast model.

A major goal of this research has been to expand the boundary-layer model, implemented by Paegle and McLawhorn (1983) and Astling et al. (1985), to include the evaporative and heat conductive effects of soil moisture. These effects of soil moisture can have a large impact on diurnal temperature changes and can thus alter the buoyancy of low-level flows such as the Great Plains nocturnal jet. The hydrology forecast model uses a two-layer-soil forecast method to predict evaporative fluxes and update soil moisture. The model allows for the addition of parameters to simulate vegetation effects such as transpiration and canopy-water evaporation.

Data from a springtime case of nocturnally-phased wind and convection were used to initialize the boundary layer model. The forecast indicated a distinct nocturanal tendency for the development of a low-level jet in the Southern Plains as well as strong rising motions along the leading edge of this wind maximum. Forecasts of nocturnal horizontal winds 500 m above Texas and Oklahoma were nearly 100% greater than daytime speeds. In addition, upward vertical velocities at night were forecast to exceed afternoon velocities by more than 4 cm s^{-1}. Overall, the timing and location of these features compared favorably with the regions of observed convection.

The model exhibits sensitivity to soil moisture. Forecast experiments were initialized with both homogeneous and heterogeneous soil distributions. In the homogeneous cases, predicted upward vertical motions over the Great Plains were decreased by almost 40% when the model was initialized with a saturated soil. It is possible that the moist soils reduced buoyant slope circulations—linked to nocturnal jet formation—by decreasing the diurnal temperature variation near the surface. The results implicated that the observed dry-soil conditions in May 1984 may have enhanced the modulation of boundary-layer convergence in the Great Plains.

Two heterogeneous soil-moisture experiments were performed to determine the necessity of detailed soil-moisture initialization in these forecasts. Strong gradients of soil moisture imposed along the slopes of the Rockies had a significant effect on the diurnal oscillation. Saturating the Plains soils increased nocturnal upward motions, whereas adding moisture to the mountains weakened rising motion. These effects may have been due to formation of a thermally-direct circulation above the boundary between wet and dry soils.

The addition of vegetation to the surface system also had some impact on response of the model. The vegetation acted to slow surface evaporation from the soil so that litle drying of the upper-soil layer occurred during the forecast. Evidently, the wetter soils damped the jet response. Little model sensitivity was observed with the addition of canopy water. Complete analysis of the effect of vegetative conditions on model performance should be deferred until a heat budget of the canopy is incorporated into the system.

The response of the boundary-layer model in these experiments demonstrated the importance of including spatial distributions of soil moisture in the forecast. Although, regular observations of soil moisture are not available, initialization procedures for an operational model could include crop moisture indices, which are observed weekly during the spring and summer. In addition, to accurately initialize many soil-moisture parameters, the question of variable soil-type specification must be addressed.

This research has examined the degree to which diurnal cycles of boundary-layer winds modulate Great Plains convection in a thunderstorm case study and in a boundary-layer model that has included the effects of soil moisture and other surface conditions. Further research should address the incorporation of a model of this type into a full-tropospheric forecast system. The impacts of upper-tropospheric phenomena, such as clouds and precipitation, as well as the effects of a changing upper-boundary condition, could be very important to the prediction of boundary-layer oscillations.

Acknowledgments. The author thanks Dr. J. Paegle of the Department of Meteorology, University of Utah, for his advice during this research. This research was supported by NSF Grants ATM841227 and ATM8611951 to the University of Utah and the Agriculture and Home Economics Experiment Station (Projects 2804 and 2841) at Iowa State University.

REFERENCES

Al Nakshabandi, G., and H. Kohnke, 1965: Thermal conductivity and diffusivity of soils as related to moisture tension and other physical properties. *Agric. Meteor.*, **2**, 179–271.

Anthes, R. A., Y. H. Kuo, S. G. Benjamin and Y. F. Li, 1982: The evolution of the mesoscale environment of severe local storms: Preliminary modeling results. *Mon. Wea. Rev.*, **110**, 1187–1213.

Astling, E. G., J. Paegle, E. Miller and C. J. O'Brien, 1985: Boundary layer control of nocturnal convection associated with a synoptic scale system. *Mon. Wea. Rev.*, **113**, 540–552.

Blackadar, A. K., 1957: Boundary layer wind maxima and their significance for the growth of nocturnal inversions. *Bull. Amer. Meteor. Soc.*, **38**, 283–290.

Bonner, W. D., 1968: Climatology of the low level jet. *Mon. Wea. Rev.*, **96**, 833–850.

Clapp, R., and G. M. Hornberger, 1978: Empirical equations for some soil hydraulic properties. *Water Resour. Res.*, **14**, 601–604.

Deardorff, J., 1977: A parameterization of ground-surface moisture content for use in atmospheric prediction models. *J. Appl. Meteor.*, **16**, 1182–1185.

Hart, J. E., G. V. van de Boogaard, J. A. Yound and J. Findlater, 1978: Aerial observations of the East African low level jet stream. *Mon. Wea. Rev.*, **106**, 1714–1724.

Hillel, D., 1980: *Fundamentals of Soil Physics.* Academic Press, 413 pp.

Holton, J. R., 1967: The diurnal boundary layer wind oscillation above sloping terrain. *Tellus*, **19**, 119–205.

McCumber, M., and R. Pielke, 1981: Simulations of the effects of heat and moisture in a mesoscale numerical model. *J. Geophys. Res.*, **86,** 9929–9938.

Mahrt, L., and H. Pan, 1984: A two-layer model of soil hydrology. *Boundary-Layer Meteorol.*, **29,** 1–20.

Matthews, E., 1985: Atlas of archived vegetation, land-use and seasonal albedo data sets. NTIS No. N8524508, NASA Technical Memorandum 86199, Goddard Space Flight Center, Institute for Space Studies, New York, 53 pp.

Means, L. L., 1952: On thunderstorm forecasting in the Central United States. *Mon. Wea. Rev.*, **80,** 165–189.

Nimah, M. N., and R. J. Hanks, 1973: Model for estimating soil water, plant, and atmospheric interrelations. I: Description and sensitivity. *Soil Sci. Soc. Amer. Proc., of America,* **37,** 522–527.

Ookouchi, Y., M. Segal, R. C. Kessler and R. A. Pielke, 1984: Evaluation of effects on the generation and modification of mesoscale circulations. *Mon. Wea. Rev.*, **112,** 2281–2292.

Paegle, J., 1984: Topographically bound low-level circulations. *Riv. Meteor. Aeronaut.*, **44,** 113–125.

——, and D. W. McLawhorn, 1983: Numerical modelling of diurnal convergence oscillations above sloping terrain. *Mon. Wea. Rev.*, **111,** 67–85.

——, W. G. Zdundowski and R. M. Welch, 1976: Implict differencing of predictive equations of the boundary layer. *Mon. Wea. Rev.*, **104,** 1321–1324.

——, J. N. Paegle, M. McCorcle and E. Miller, 1984: Diagnoses and numerical simulation of a low-level jet during ALPEX. *Beitr. Phys. Atmos.*, **57,** 419–430.

Pan, H.-L., and L. Mahrt, 1987: Interaction between soil hydrology and boundary-layer development. *Bound.-Layer Meteor.* **38,** 185–202.

Penman, H. L., 1948: Natural evaporation from open water, bare soil and grass. *Proc. Roy. Soc.* **A193,** 120–195.

Pitchford, K. L., and J. London, 1962: The low level jet as related to nocturnal thunderstorms over Midwest United States. *J. Appl. Meteor.*, **1,** 43–47.

Shuman, F. G., 1957: Numerical methods in weather prediction. II: Smoothing and filtering. *Mon. Wea. Rev.*, **85,** 357–361.

Smagorinsky, J., 1963: General circulation experiments with the primitive equations. I: The basic experiment. *Mon. Wea. Rev.*, **91,** 99–164.

Wallace, J. M., 1975: Diurnal variations in precipitation and thunderstorm frequency over the conterminous United States. *Mon. Wea. Rev.*, **103,** 406–419.

Zdunkowski, W. G., J. Paegle and J. P. Reilly, 1975: The effect of soil moisture upon the atmosphere and soil temperature near the air-soil interface. *Arch. Meteor. Geophys. Bioklim.* **24,** 245–268.

Zinke, P. J., 1967: Forecast interception studies in the United States. *Forest Hydrology,* W. E. Sopper and H. W. Lull, Eds., Pergamon, 137–161.